Front. Optoelectron. China 2008, 1(1–2): 44–49
DOI 10.1007/s12200-008-0055-8

RESEARCH ARTICLE

Overcoming ill-posedness of diffuse optical tomography in steady-state domain

Guotao QUAN, Kun BI, Shaoqun ZENG, Qingming LUO (✉)

The Key Laboratory of Biomedical Photonics of Ministry of Education, Huazhong University of Science and Technology, Wuhan 430074, China

Abstract In recent decades, diffuse optical tomography (DOT) has drawn more and more interest in molecular imaging because of its advantage of large penetration depth in optical image technology. However, ill-posedness problems have dramatically limited this application technique. In this paper, a new method to remove the ill-posedness of DOT is introduced. With a rotating steady-state domain experiment system, by increasing experimental data that could be obtained from any visual angle, four contrast experiments were simulated. It was proved that when the sum of the experiment data is larger than that of the unknown optical coefficient of phantom, ill-posedness would be reduced and the quality of the reconstructed image could be improved.

Keywords diffuse optical tomography (DOT), ill-posedness, diffusion approximation, rotation DOT system

1 Introduction

Diffuse optical tomography (DOT) is a fast growing research field in which near-infrared light is used for imaging internal body structures. More and more instruments of DOT with sensitive light transmission measurements are available nowadays [1–3]. Several algorithms that can transform these measurements into useful cross-sectional images have matured so that first clinical trials have become possible, especially in breast imaging [4,5]. However, a big obstacle in DOT is that the image reconstruction problem is ill-posed or underdetermined. Because reconstruction algorithms want to regenerate the inner 2D properties of the medium from the 1D measurement, plenty of different distributions of the optical properties inside the medium will lead to the same set of detector readings on the surface of the medium.

Received July 30, 2007; accepted December 24, 2007

E-mail: qluo@mail.hust.edu.cn

Most researchers pay attention to getting pre-experiment information combined with different imaging modalities, such as MRI, X-CT, and others, to reduce the ill-posedness of DOT [6]. However, in this case, the independence of the DOT system will be reduced, and the cost of the DOT system will increase, as the DOT system must work with other imaging modality. In this paper, the ill-posedness of DOT was conquered in a new way, by which no pre-experiment knowledge should be introduced. To turn the ill-posedness problem into a determined problem, more experimental data were imported. To get any experiment data, a new rotating experiment system based on charge coupled device (CCD) and continuous light source was developed, with which more experiment data could be obtained from any visual angle according to the DOT reconstruction algorithm.

In this paper, first, the basic theory of DOT arithmetic is introduced in detail. A brief introduction of the system is given. Finally, the contrasting experiment results are presented to prove the validity of this method.

2 Theory

The photon transport in tissue can be mathematically described by the particle transport equation, which has been given by Duderstadt and Martin. The particle transport equation applied to photons is also called the equation of radioactive transfer [7–10]. In this equation, if $\mu_a(\boldsymbol{r}) \ll \mu_s(\boldsymbol{r})$, $\mu_a(\boldsymbol{r})$ and $\mu_s(\boldsymbol{r})$ are the absorbing and scattering parameter of the tissue with the units of cm^{-1} respectively, the radioactive transfer equation can be rewritten as the diffusion approximation equation, which can be quickly solved compared to the radioactive transfer equation [11]

$$\nabla\cdot[D\nabla\Phi(\boldsymbol{r})]+\mu_a(\boldsymbol{r})\Phi(\boldsymbol{r})=0, \tag{1}$$

and the Robin boundary condition is

$$2\rho D(\boldsymbol{r})\frac{\partial}{\partial \boldsymbol{n}}\Phi(\boldsymbol{r})+\Phi(\boldsymbol{r})+S(\boldsymbol{r})=0, \tag{2}$$

where $\Phi(\boldsymbol{r})$ represents the photon intensity, with units of W/cm^2, $\boldsymbol{n}$ is outward normal of the tissue surface. $D(\boldsymbol{r})$ is the reduced transport coefficient, which could be also expressed as

$$D(\boldsymbol{r})=[3(\mu_a+(1+g)\mu_s)]^{-1}, \tag{3}$$

where g is anisotropy factor.

There are several methods that can solve this diffusion equation, such as finite differential method (FDM), finite element method (FEM), and Monte Carlo (MC) method, but only FEM could be used in complex boundary condition and quickly solve the diffusion equation.

With FEM, the regions of tissue can be discretized into n_e elements ($\Omega_1, \Omega_2,\ldots,\Omega_{n_e}$) and n_v nodes ($n_1, n_2,\ldots n_{n_v}$), and $\Phi(\boldsymbol{r})$ can be expressed with piecewise polynomial interpolation functions [12–14] as

$$\Phi=\sum_{i=1}^{n_v} c_i\psi_i. \tag{4}$$

With the FEM, Eqs. (1) and (2) could be formulated into the following matrix form as

$$(\boldsymbol{A}+\boldsymbol{C}+\boldsymbol{Q})\Phi=\boldsymbol{H}, \tag{5}$$

where

$$\boldsymbol{A}(i,j)=\int_\Omega D(\boldsymbol{r})\left[\nabla\psi_i(\boldsymbol{r})\cdot\nabla\psi_j(\boldsymbol{r})\right]\mathrm{d}\boldsymbol{r}, \tag{6}$$

$$\boldsymbol{C}(i,j)=\int_\Omega \mu_a(\boldsymbol{r})\psi_i(\boldsymbol{r})\psi_j(\boldsymbol{r})\mathrm{d}\boldsymbol{r}, \tag{7}$$

$$\boldsymbol{Q}(i,j)=\frac{1}{2\rho}\oint_\Omega \psi_i(\boldsymbol{r})\psi_j(\boldsymbol{r})\mathrm{d}\boldsymbol{r}, \tag{8}$$

$$\boldsymbol{H}(i,j)=-\frac{1}{2\rho}\oint_\Omega S(\boldsymbol{r})\psi_i(\boldsymbol{r})\mathrm{d}\boldsymbol{r}. \tag{9}$$

Combining Eq. (5), which shows the result of photon intensity in theory, with experiment data, an object function $F(D,\mu_a)$ which depends on the reduced transfer coefficient D and absorbing coefficient μ_a [15–17] could be formulated as

$$F(D,\mu_a)=\frac{1}{2}\left[\frac{\Phi_{mes}-\Phi_{theo}(D,\mu_a)}{\Phi_{mes}}\right]^2, \tag{10}$$

where Φ_{mes} stands for the experiment measurement on the boundary, and Φ_{theo} represents the calculation on the boundary in theory.

The setting of D and μ_a will be the best values which proximally equal to the real values of the tissue optical coefficients, under the condition that the minimal value of the object function $F(D,\mu_a)$ is achieved.

3 Experiment system

A new DOT experiment system with rotating style [18–20] was designed, which consist of a digital camera, laser source (650 nm), motorized rotation stage, linear stage, data link mode and CCD. The laser source was mounted on the linear stage which carried the source to various positions along it. The rotation stage carried the camera and the linear stage in a line so that the camera could take images at various angles. The phantom was placed at the center between the CCD and laser source. Without any fibers and optical switch, the DOT system is compact and can easily be operated. Figure 1(a) shows the system's construction.

Following Firbank M's instruction [21], a stable and reproducible phantom for DOT experiment was made with two glass sticks inserted in as the heterogeneity. Figure 2 shows the experiment phantom, and sequence images at an interval of 5.625° would be obtained.

4 Results and discussion

Figures 3 and 4 show the corresponding positions of the glass sticks (horizontal black lines) in phantom. As the phantom is made from resin, its optical parameter is not so sensitive to X-ray yet sensitive to near-infrared light; therefore, it seems to be translucent in X-ray imaging, but not in DOT reconstructed imaging. The vertical black line represents the slice that will be reconstructed by DOT. The radius of the phantom is 1.31 cm, and the radius of the glass stick is 0.35 cm. According to the topology, FEM was utilized to mesh the phantom geometry, which divided the phantom geometry into 374 nodes and 682 elements, as shown in Fig. 5.

Figure 1(b) shows the initial position of the light source and suppositional detectors. In this experiment, the CCD was used to detect the photons, and one pixel in CCD imaging represented a signal suppositional detector. However, it is unnecessary to choose all pixels in CCD imaging to reconstruct the optical property, as it would cost lots of time, so only a few suppositional detectors were chosen. Because of the rotation of the system, the positions of the light source and suppositional detectors would change a little, which would supply a new setting of experiment data.

Four contrast experiments with the same geometry mesh had been practiced. The only difference between them is the sum of the experiment data. In the first

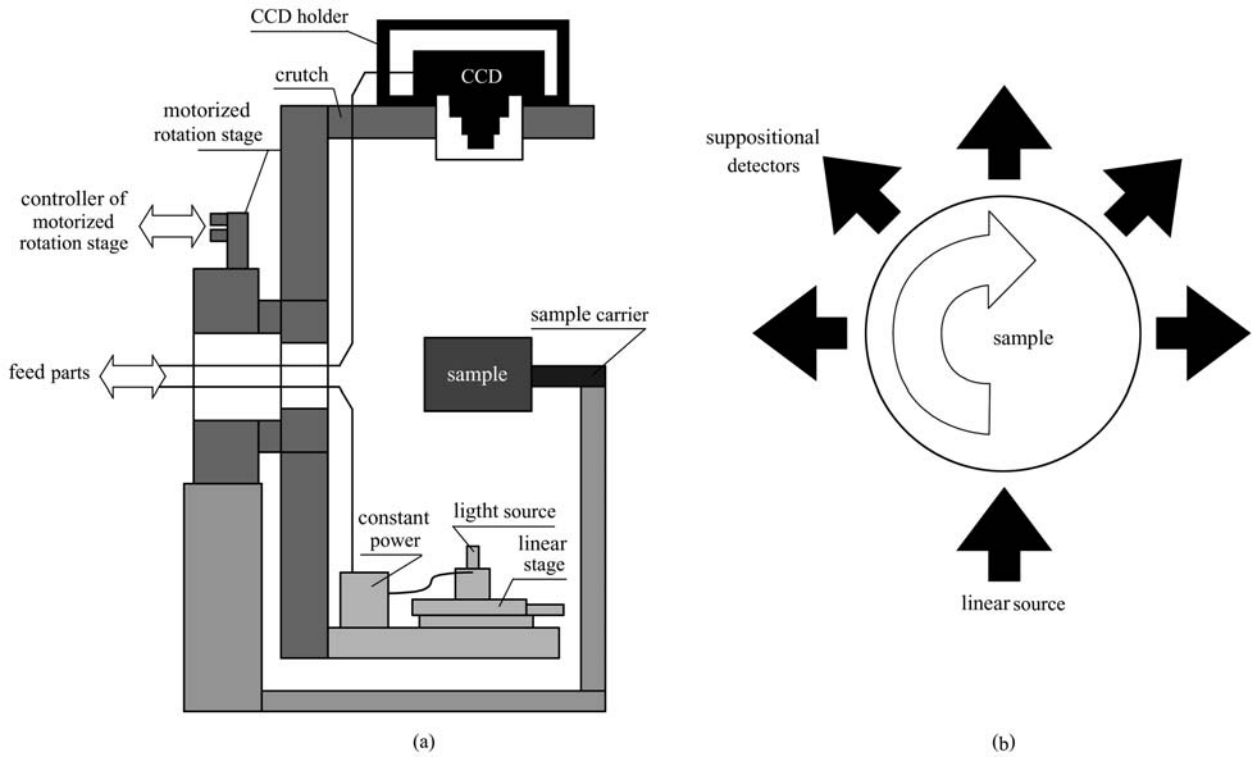

Fig. 1 Steady state DOT system. (a) Construction of DOT system; (b) positions of light source and the suppositional detectors

experiment, images are taken at an interval of 22.5°, namely the light sources with 16 positions was introduced in the experiment. 8 little areas that contain few pixels in the image taken by CCD have been captured in each image. There are 8 assumed detectors corresponding to the 8 areas, so there were 16 light sources and 8 suppositional detectors corresponding to each light source position.

In the second experiment, there were 32 light sources and 16 suppositional detectors corresponding to each light source position. In the third experiment, there were 32 light sources and 32 suppositional detectors corresponding to each light source position. In the fourth experiment, there were 32 light sources and 64 suppositional detectors corresponding to each light source position.

Fig. 2 Experiment phantom

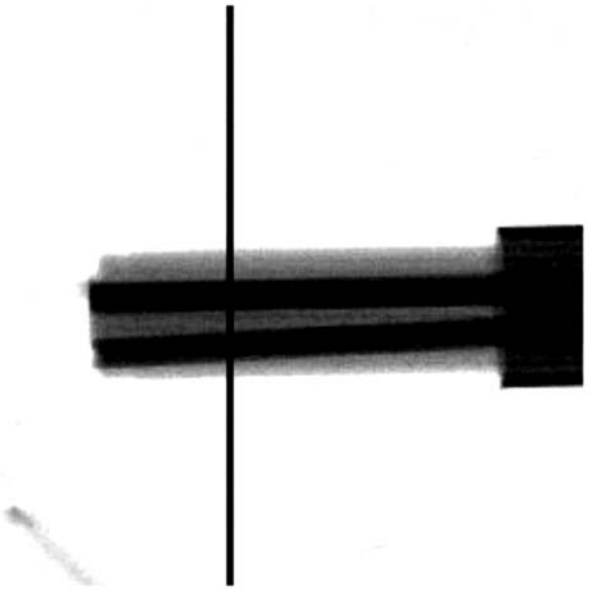

Fig. 3 Planform of the phantom irradiated by X-ray

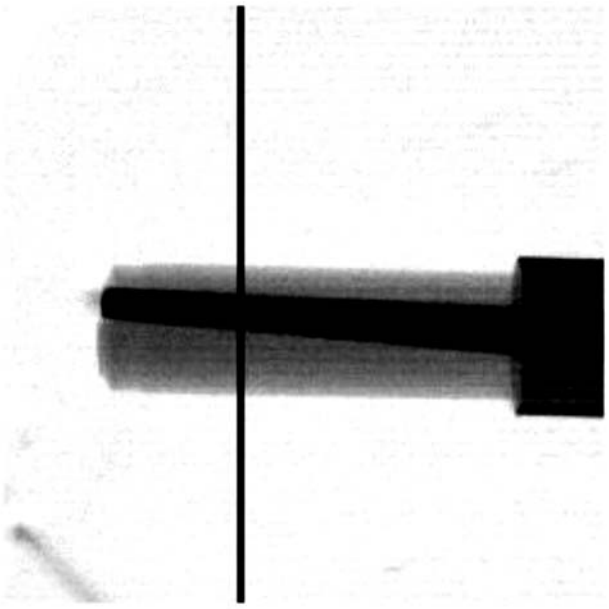

Fig. 4 Side elevation of the phantom irradiated by X-ray

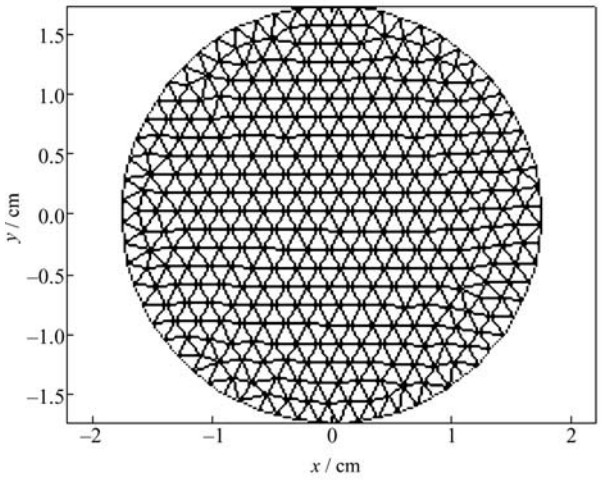

Fig. 5 Mesh of one slide of the phantom

In the first experiment, the sum of the experiment data was about $16 \times 8 = 128$, but there were 374 reduced transport coefficients and 374 absorbing coefficients to be solved. In other words, there were $374 \times 2 = 748$ variables but only 128 equations, which made this problem become ill-posed. Figures 6 and 7 show the results of this experiment, and the two heterogeneities could not be found.

In the second experiment, the sum of the experiment data was about $32 \times 16 = 512$, the problem was also ill-posed. Figures 8 and 9 show the results of this experiment. Although the two heterogeneities could be found in Fig. 8, as the pre-experiment knowledge, the absorbing coefficients of the glass sticks had little difference between its background matter, so the results were also bad.

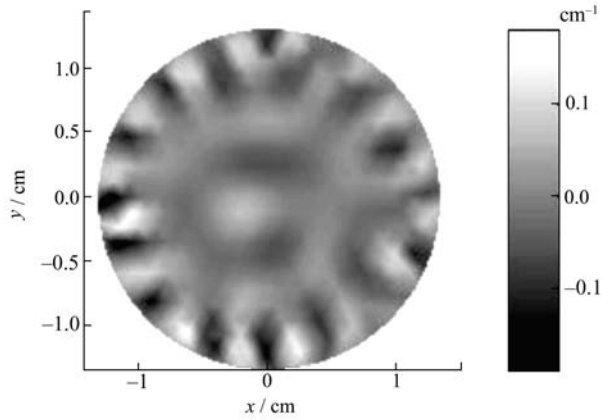

Fig. 6 Absorbing property image with 16 light sources position and 8 suppositional detectors

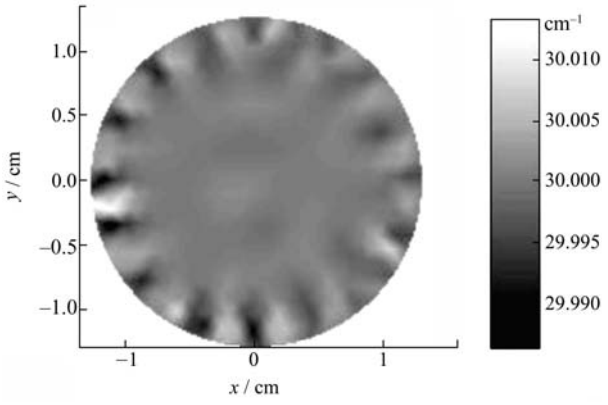

Fig. 7 Scattering property image with 16 light sources position and 8 suppositional detectors

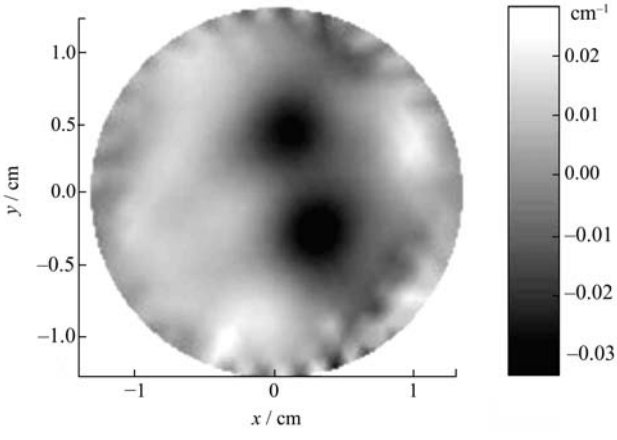

Fig. 8 Absorbing property image with 32 light sources position and 16 suppositional detectors

In the third experiment, the sum of the experiment data was about $32 \times 32 = 1024$, in which the ill-posedness had been successfully reduced. Figures 10 and 11 show the results of this experiment. The two heterogeneities could be clearly found in Fig. 11. Compared to Figs. 3 and 4,

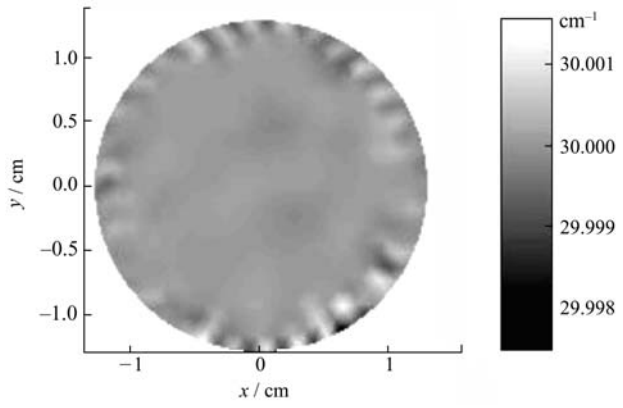

Fig. 9 Scattering property image with 32 light sources position and 16 suppositional detectors

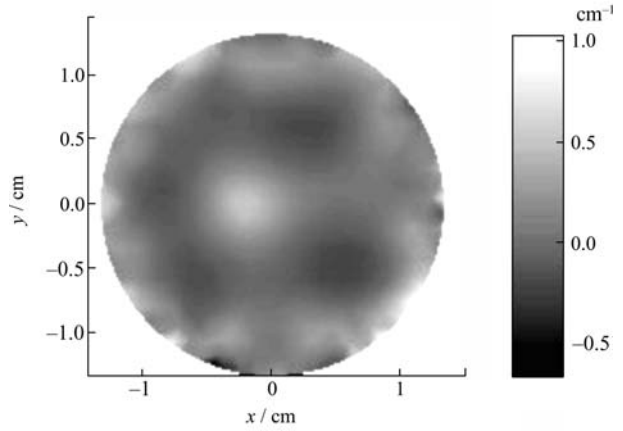

Fig. 10 Absorbing property image with 32 light sources position and 32 suppositional detectors

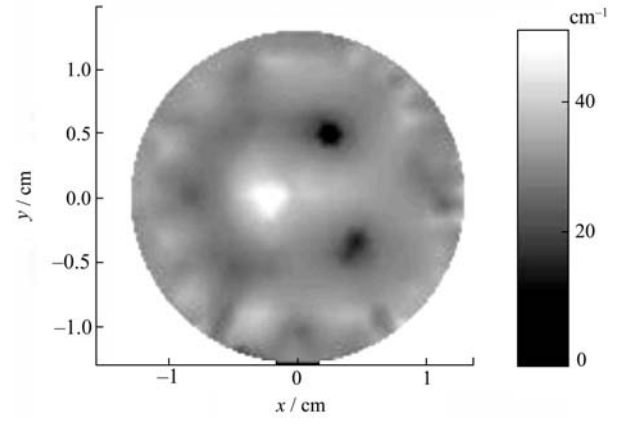

Fig. 11 Scattering property image with 32 light sources position and 32 suppositional detectors

the positions of two heterogeneities were almost the same as the real situation, according with the pre-experiment knowledge, in which the scattering coefficient of the heterogeneities distinguished was different from that of the background matter, and the absorbing coefficient of the heterogeneities was almost the same as that of the background matter.

In the fourth experiment, the sum of experiment data is about $32 \times 64 = 2048$, which also made the problem certain. Figures 12 and 13 show the results of this experiment, which are pretty well compared to the results of the third experiment.

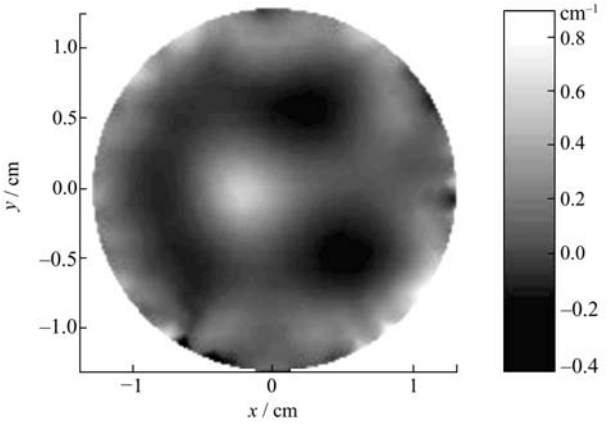

Fig. 12 Absorbing property image with 32 light sources position and 64 suppositional detectors

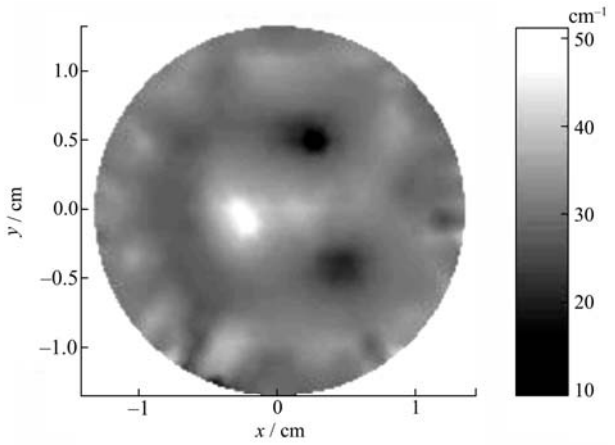

Fig. 13 Scattering property image with 32 light sources position and 64 suppositional detectors

In the first and second experiments, the sum of the experiment data is less than that of the unknown optical coefficients, while in the third and fourth experiments, the sum of the experiment data is larger than that of the unknown optical coefficients. The results of the third and fourth experiments are better than that of the first and second experiments, therefore the degree of the ill-posedness of DOT decreases as the sum of experiment data increases. In this way, the ill-posedness of DOT can be reduced without any pre-experiment knowledge from other imaging modality, such as MRI X-CT and so on.

5 Conclusions

In this paper, a new method to overcome the ill-posedness of DOT was presented. By utilizing this experiment scheme and algorithm, the interval of the rotation stage could be adjusted to obtain adequate measurement data, with which the ill-posedness of DOT reconstruction could be reduced. The four contrast experiments indicated the bright application future of this kind of experiment schema and algorithm.

Acknowledgements This research was supported by the National Natural Science Foundation of China (Grant Nos. 30470460 and 90508003) and 863 Project (No. 2006AA020801).

References

1. Wells K, Hebden J C, Schmidt F E W, et al. The UCL multi-channel time-resolved system for optical tomography. In: Chance B, Alfano R R, eds. Optical Tomography and Spectroscopy of Tissue: Theory, Instrumentation, Model, and Human Studies II. San Jose: SPIE, 1997, 2979: 599–607
2. van Houten J P, Benaron D A, Spilman S, et al. Imaging brain injury using time-resolved near infrared light scanning. Pediatric Research, 1996, 39(3): 470–476
3. Miwa M, Ueda Y. Development of time-resolved spectroscopy system for quantitative noninvasive tissue measurement. In: Chance B, Alfano R R, eds. Optical Tomography, Photon Migration, and Spectroscopy of Tissue and Model Media: Theory, Human Studies, and Instrumentation. San Jose: SPIE, 1995, 2389: 142–149
4. Ntziachristos V, Ripoll J, Wang L H, et al. Looking and listening to light: the evolution of whole-body photonic imaging. Nature Biotechnology, 2005, 23(3): 313–320
5. Franceschini M A, Moesta K T, Fantini S, et al. Frequency-domain techniques enhance optical mammography: initial clinical results. Proceedings of the National Academy of Sciences of the United States of America, 1997, 94(12): 6468–6473
6. Hielscher A H, Bartel S. Overcoming ill-posedness in optical tomography. In: Hanson K M, ed. Medical Imaging 2000: Image Processing. San Diego: SPIE, 2000, 3979: 575–585
7. Abdoulaev G S, Hielscher A H. Three-dimensional optical tomography with the equation of radiative transfer. Jounal of Electronic Imaging, 2003, 12(4): 594–601
8. Wright S, Schweiger M, Arridge S R. Solutions to the transport equation using variable order angular basis. In: Kai Licha, Rinaldo Cubeddu, eds. Photon Migration and Diffuse-Light Imaging II. Munich: SPIE, 2005, 5859: 585914.1–585914.8
9. Ren K, Abdoulaev G S, Bal G, et al. Algorithm for solving the equation of radiative transfer in the frequency domain. Optics Letters, 2004, 29(6): 578–580
10. Tarvainen T, Vauhkonen M, Kolehmainen V, et al. Finite element model for the coupled radiative transfer equation and diffusion approximation. International Journal for Numerical Methods in Engineering, 2006, 65(3): 383–405
11. Arridge S R. Optical tomography in medical imaging. Inverse Problems, 1999, 15(2): 41–93
12. Schweiger M, Arridge S R, Hiraoka M, et al. The finite element method for the propagation of light in scattering media: Boundary and source conditions. Medical Physics, 1995, 22(11): 1779–1792
13. Cong A X, Wang G. A finite-element-based reconstruction method for 3D fluorescence tomography. Optics Express, 2005, 13(24): 9847–9857
14. Lee J H, Kim S, Kim Y T. Finite element method for diffusive light propagations in index-mismatched media. Optics Express, 2004, 12(8): 1727–1740
15. Arridge S R, Schweiger M. Photon-measurement density functions part 2: finite-element-method calculations. Applied Optics, 1995, 34(34): 8026–8037
16. Roy R, Sevick-Muraca E M. Truncated Newton's optimization scheme for absorption and fluorescence optical tomography: part I theory and formulation. Optics Express, 1999, 4(10): 353–371
17. Roy R, Sevick-Muraca E M. Truncated Newton's optimization scheme for absorption and fluorescence optical tomography: part II reconstruction from synthetic measurements. Optics Express, 1999, 4(10): 372–382
18. Ntziachristos V, Weissleder R. Charge-coupled-device based scanner for tomography of fluorescent near-infrared probes in turbid media. Medical Physics, 2002, 29(5): 803–809
19. Mahmood U, Tung C, Bogdanov A, et al. Near-infrared optical imaging system to detect tumor protease activity. Radiology, 1999, 213(3): 866–870
20. Benaron D A, Hintz S R, Villringer A, et al. Noninvasive functional imaging of human brain using light. Journal of Cerebral Blood Flow & Metabolism, 2000, 20(3): 469–477
21. Firbank M, Oda M, Delpy D T. An improved design for a stable and reproducible phantom material for use in near-infrared spectroscopy and imaging. Physics in Medicine and Biology, 1995, 40(5): 955–961